Version of Record: https://www.sciencedirect.com/science/article/pii/S0260877421000091
Manuscript_f876f55e1ff7231084c8de3272a23796

Microstructure analysis of crust during deep-fat or hot-air frying to understand French fry texture.

Têko Gouyo [a, c], Eric Rondet [c], Christian Mestres [b, c], Céline Hofleitner [a], Philippe Bohuon [c*]

[a] SEB, Ecully Food Science; 112 Chemin du Moulin Carron, 69130 Écully

[b] CIRAD, UMR QualiSud, Montpellier, France.

[c] QualiSud, Univ Montpellier, Institut Agro, CIRAD, Univ d'Avignon, Univ de La Réunion, Montpellier, France.

* Corresponding author: Philippe Bohuon, Montpellier SupAgro, UMR QualiSud, 1101 av. Agropolis, F-3409 Montpellier, France. Tel. +33 467 87 40 81; Fax: +33 467 61 44 44. E–mail address: philippe.bohuon@supagro.fr

Abstract

This study aimed to identify the microstructural parameters of the crust that are responsible for the crispness of French fries. The French fry microstructure was visualized by

© 2021 published by Elsevier. This manuscript is made available under the CC BY NC user license
https://creativecommons.org/licenses/by-nc/4.0/

X-ray micro-computed tomography (XMT). Analysis of the images provided information on the pore size distribution, global porosity of the French fries and local porosity of the crust region. The results revealed that prefrozen French fries do not practically undergo any volume shrinkage during frying. The total porosity created in French fries corresponds to the volume of water loss during frying. The difference between hot-air fried and deep-fat fried French fries was mainly related to the pore diameter and pore size distribution in the crust. Principal component analysis between the sensory and morphometric parameters showed that the volume of small pores (diameter < 0.15 mm) and the span of the pore size distribution in the first millimetres of the crust correlated with the crispness of the product ($r > 0.85$, P value < 0.05). Thus, a French fry is crispier if the pores generated in the crust have a small median diameter (diameter < 0.2 mm), as well as a large dispersion of pore diameters.

Highlights (maximum 85 characters)

- The French fry crust microstructure revealed by XMT is linked to crispness defined by sensory analysis
- The total porosity created in pre-frozen French fries corresponds to water loss
- A higher porosity in the crust generally results in a higher perceived crispness
- A small pore diameter and heterogeneous pore size distribution in the crust improve the crispness

Keywords

French fries; Crispness; Crust microstructure; X-ray micro-computed tomography, sensory analysis

1. Introduction

French fries are a specific solid with a moist and soft core and a crispy outer dry crust of approximately 0.5 — 1.5 mm (Bouchon and Aguilera, 2001; Pedreschi and Aguilera, 2002; van Koerten et al., 2015). French fries are popular potato products in many countries because of their attractive texture. Texture is one of the important quality aspects, and a crispy crust is an important factor in the sensory properties of French fries (Vickers and Bourne, 1976; Pedreschi and Aguilera, 2002; Salvador et al., 2009). During potato frying, the formation of the crust is the result of changes in the native potato structure caused by heat and mass transfer (Pedreschi and Aguilera, 2002; Pedreschi, 2009). The structure of the core and crust of a fried product is affected by the time-temperature couple and the frying process, resulting in different types of fried products. The transformations during frying determine the microstructural properties of the crust, such as porosity, pore size shape and pore distribution (Bouchon and Aguilera, 2001; Dalen et al., 2007; Ziaiifar et al., 2010; van Koerten et al., 2015). The microstructure of the crust determines the sensory characteristics of the French fry (Aguilera, 2005; Dalen et al., 2007; van Koerten et al., 2015).

In the last decade, hot-air fryers have been developed to overcome the high oil uptake during the frying process with conventional fryers (deep-fat frying). The objective is to reduce fat consumption from French fries. The current disadvantage of this type of fryer is less intense heat and mass transfer, generating French fries with less crispness compared to those obtained by deep-fat frying (Teruel et al., 2015; Gouyo et al., 2020). The most important critical contributors to the physical and rheological behaviour, texture and sensory characteristics of fried food products have sizes in the range of 100 µm (Aguilera, 2005). Knowing how these elements are arranged and interact with the sensory quality of food can contribute to process optimization (Dalen et al., 2007).

In the literature, several techniques have been used to study the microstructural changes in food products. These include mercury porosimetry and pycnometry, which represent experimental methods commonly used to quantify the porosity and density of materials (Kassama and Ngadi, 2005; Rahman et al., 2002). Several other techniques have been used, including microscopy (Kaláb et al., 1995; Ferrando and Spiess, 2000; Hesso et al., 2015), magnetic resonance imaging (Horigane et al., 2003; Lucas et al., 2018), computer vision techniques (Hullberg and Ballerini, 2003; Du and Sun, 2006), and most recently, X-ray micro-computed tomography (XMT) (Léonard et al., 2008; Laverse et al., 2011; Adedeji et al., 2011; Hafsa et al., 2014; van Koerten et al., 2015). In XMT, product components are differentiated according to their ability to absorb X-rays, which is directly correlated to their density. The advantage of the latest technique compared to the others is that the XMT is noninvasive, nondestructive and follows a basic sample preparation procedure that does not affect the sample (Adedeji et al., 2011; Alam and Takhar, 2016). The results of XMT analysis provide high-resolution 3D visualization (on the order of a few micrometers according to the apparatus resolution), allowing visualization of the internal morphology of the samples and quantification of the morphometric properties (structure, size, etc.).

In recent years, many studies have used XMT to study the internal morphological configuration of many fried food products: deep-fat fried breaded chicken nuggets (Adedeji et al., 2011), deep-fat fried coated chicken nuggets (Adedeji and Ngadi, 2011), deep-fat-fried chicken meat (Kassama and Ngadi, 2005), and bread crumbs (Primo-Martín et al., 2010; Altamirano-Fortoul et al., 2012; Besbes et al., 2013). In the case of French fried potatoes, a few studies have focused on their microstructure. Among them, van Koerten et al. (2015) studied the impact of operating variables (cooking time and temperature) on the structural properties of French fries. In this latest study, the water losses were very low (< 35%) and far from the values that allowed the production of crispy French fries (water loss > 45%

according to Gouyo et al. (2020)). Some others, such as Vauvre et al. (2014) and Alam and Takhar, (2016), have also used XMT to better understand the impact of the microstructure characteristics on the oil uptake during deep-fat frying. (sur des frites? Autre chose? À préciser).

The objective of this study was to identify the morphometric parameters of the microstructure of the crust by XMT, which can explain the texture of French fries. Analysis of the images provided information on the pore size distribution, global porosity of the French fries and the gradient porosity of the crust region. A quantitative descriptive analysis was performed to evaluate sensory parameters. An instrumental texture analysis (acoustics and force-deformation test) was also performed. The relationships between the morphometric, sensory and instrumental parameters were established. Finally, this approach was used to compare two products with contrasting textures generated by deep-fat frying and hot-air frying.

2. Materials & Methods

2.1. Raw materials

The experiments were carried out with frozen French fries (Mc-Cain Tradition, made in Harnes, France, with French potatoes) stored in a cold room at –18 °C until use. The fries were resized to 60 mm in length and 9 mm in thickness (9×9×60 mm). A specific fry cutter was used to cut the frozen French fries.

2.2. Frying equipment

Two main fryers were used: a commercial deep-fat fryer (Filtra One FF162100 Seb) with a power of 1900 W, a frying capacity of 1.20 kg of French fries and an oil volume of 2.10 L and hot-air frying equipment (Airrer Philips XL HD9240/90, Avance Collection, Amsterdam, The Netherlands) with a power of 2100 W and a frying capacity of 1.20 kg of

French fries. To determine the amount of moisture evaporated from the potatoes during frying, the fryers were placed on a balance (Sartorius CPA34001S, France, with a capacity of 34 kg for 10^{-4} kg of sensibility) that allowed continuous recording of the water loss.

2.3. Sample preparation

The sample preparation aimed to produce samples with different contrasting structures. Each experiment was performed with 0.300 kg of calibrated French fries. Different levels of water loss were obtained ranging from 0% to 60%. The water loss was defined as the mass (kg) or the volume (m^3) of water lost during frying divided by the initial mass (i.m., kg) or the volume (m^3) of the frozen French fries before frying (WL in kg water/kg of fries or m^3 of water/m^3 of fries). The samples were coded according to their frying conditions, as shown in Table 1. After frying, the middle part of the French fry was cut (9×9×30 mm) and soaked in petroleum ether for 30 seconds to remove most of the oil (this treatment increases the resolution of the XMT images) and then rapidly scanned by XMT. The waiting time from the end of the frying to the XMT analysis was estimated to be an average of 5 to 10 minutes.

2.4. XMT scan parameters

A volume of 9×9×30 mm^3 of French fry sample was scanned in a SkyScan 1272 (Bruker µCT, Kontich, Belgium) at a nominal resolution (pixel size) of 11.5 microns employing an aluminium filter 0.25 mm thick. The applied X-ray tube voltage was 42 kV, and the current intensity was 20 µA. Camera pixel binning of 3×3 was applied. The scan orbit was 360 degrees with a rotation step of 0.7 degrees for a scan duration of 23 minutes. The scans were carried out in triplicate with one French fry per test.

2.5. Image reconstruction

Reconstruction was carried out with a modified Feldkamp (Feldkamp et al., 1984) algorithm using SkyScan™ NRecon software (Version: 1.7.1.0, Bruker µCT, Kontich, Belgium) accelerated by GPU (Yan et al., 2008). Gaussian smoothing, ring artefact reduction and beam hardening correction were applied. The reconstruction of each sample produced a series of 845 cross-sections of 896 × 1344 pixels.

2.6. Region of interest selection

Region of interest selection, segmentation to binary and morphometric analysis were all performed using SkyScan CT-Analyser ("CTAn") software (Version: 1.17.7.2, Bruker µCT, Kontich, Belgium). The "ROI shrink-wrap" function was used to select the region of interest (ROI). This step was used to adjust to the surface or contour line of the fry. The same ROI was analysed for all the samples. It was selected in the center of the reconstructed images to eliminate any edge effects, artefacts and damage from sample cutting. The ROI corresponded to 12 mm of French fries and was composed of 500 stacks (2D images).

2.7. Image segmentation to binary and morphometric analysis

Global thresholds were selected by the Otsu algorithm (Otsu, 1979) to segment the image to binary. The same global threshold values were applied to all the measured samples. The 3D morphometric parameters were calculated over the total volume of the French fry and on the crust volume. Noise objects were removed from the binarised image by despeckle morphological operations in CTAn. The porosity was determined as the percentage of voxels segmented as pores to the total number of voxels (void + solid) (Primo-Martín et al., 2010). The morphometric parameters in 3D were based on the analysis of a marching cubes-type model (Lorensen and Cline, 1987) with a rendered surface. The pore size in 3D was calculated using the local thickness or "sphere-fitting" (double distance transform) method (Borgefors, 1996; Hildebrand and Rüegsegger, 1997; Remy and Thiel, 2002). For the crust analysis, a morphological 2D erosion-type operation was performed with a defined radius

corresponding to the required crust thickness. Erosions with radii of 43.5, 61 and 87 were used for crust sections with thicknesses of 0.5 mm, 0.7 mm and 1 mm, respectively (Figure 1 b and c). From the pore size distribution, morphometric parameters such as the pore volume (V_p) of different pore sizes (V_p[0 to 0.15 mm], V_p[0.15 to 0.32 mm] and V_p[0.32 to 0.5 mm]), median diameter (d_{50}) and span $= (d_{90} - d_{10}) / d_{50}$ were estimated.

2.8. Sensory analysis

The descriptive sensory analysis data of Gouyo et al., (2020) for five samples with contrasting textures (Table 1) were used. Two samples were produced with a conventional deep-fat fryer with water losses of 50 and 60% (i.m.) (DF180_50 and DF180_60, respectively). Three other samples were obtained by hot-air frying at 180 or 200 °C with water losses of 50 and 60% (i.m.) (AY180_50, AY180_60 and AY200_50, respectively). Four sensory descriptors were considered (crispiness of the crust, product hardness, softness of the core and floury of the core).

2.9. Instrumental texture analysis

The mechanical (penetration test) and acoustic analysis data of Gouyo et al., (2020) for five samples with contrasting textures (Table 1) were also used. The following parameters — maximum force (Fmax, N) and number of sound peaks (NSP)— were used to characterize the product hardness and crispiness of the crust, respectively.

2.10. Statistical analysis

The statistical analysis of the results was carried out using XLSTAT version 2017 (ANOVA, Student's t-test and PCA test). The ANOVA procedure at a significance level of 0.05 and the Tukey test and Student's t-test were applied to assess the significant differences between the investigated parameters. Principal component analysis (PCA) of correlation was also conducted. The sensory and instrumental data were plotted as active variables, and the morphometric data were plotted as supplementary variables.

3. Results and discussion

3.1. Image description

Cross-sectional slices of the XMT scans for different water losses are shown in Figure 2. Overall, the shape of the French fries do not change much. The square section (9×9 mm) is well preserved during frying, but the porosity of the fries increases with increasing water loss. At the end of frying, the French fries have three distinct regions: a peripheral crust, a very porous zone that surrounds the central region, and a core. For the WL = 0% sample, it can be observed that there is already an initial structure with an existing pre-crust that has already formed as a result of the pretreatment of the frozen French fries. This peripheral precrust consists of a single layer of porous bubbles with an approximate diameter of 0.1 mm. Figure 2 also shows that it is difficult to distinguish the boundaries of the crust region. The thickness of the crust differs greatly according to the water loss and also according to the French fry zone considered. For example, for a French fry with WL = 60% (Figure 2 a), the crust thickness of the left part of the image is smaller (0.2 to 0.5 mm) than the crust thickness of the right part (0.5 to 1.5 mm). Figure 2b shows that the crust of deep-fat fries is filled with oil (light grey). Despite the soaking of French fries in petroleum ether for 30 seconds, there is still visible oil in the pores of the crust. This residual oil was removed during thresholding. By simple observation, it is difficult to differentiate deep-fat fries from the hot-air fries in Figure 2.

3.2. Total porosity and volume change

Figure 3 shows the evolution of the total volume and the porosity created in the French fries as a function of water loss for the hot-air and deep-fat fries. The relative uncertainty between replicates is quite low (1.5% to 6%), and there is no significant evolution (P value > 0.05) in the total volume during frying (Figure 2 and Figure 3 a)); the frozen French fries are not subjected to any significant volume shrinkage (< 7%) when

dehydrated during frying, even at high water loss (WL = 60%). This is not the case when the raw material is native potatoes. Several studies carried out on frying raw potatoes showed a significant shrinkage of the volume of French fries (30 to 40% of the initial volume) during frying (Krokida et al., 2000; Costa et al., 2001; Yamsaengsung and Moreira, 2002).

The total porosity of the French fries was analysed for different water losses. The porosity is defined as the ratio of the cumulative volume of all the pores created relative to the total volume of the analysed French fry (Figure 3 b). The relative uncertainty between replicates is also quite low (2% to 20%), and for the same water loss, the total porosities created in the French fries obtained by deep-fat frying or hot-air frying are not significantly different (P value > 0.05); the porosity created in the fry indeed increases proportional to the water loss of the product independent of the frying condition (hot-air or deep-fat frying). The volume of the water lost during the frying operation corresponds to 92 ± 15% and 93 ± 13% of the pore volume created during hot-air frying and deep-fat frying, respectively, thus confirming the lack of volume shrinkage. The measured porosity values are higher than the orders of magnitude mentioned in the literature. For example, for a water loss of 30%, the measured porosity is 28%, whereas Pinthus et al. (1995) obtained 20% and van Koerten et al. (2015) 12% porosity for the same water loss. This can be explained by the significant shrinkage of the French fry in these studies that were performed with raw potatoes, whereas we used frozen French fries.

3.3. Porosity of the crust

To understand the microstructural phenomena that affect the texture of deep-fat and hot-air French fries, an analysis of the crust zone of French fries was carried out. The main difficulty in the analysis of the crust of the French fry is the delimitation of the geographical zone that corresponds to the crust. Several studies in the literature defined the crust as the superficial porous region (completely dry layer of a fried potato) without defining a specific

thickness (Miranda and Aguilera, 2006; Ziaiifar et al., 2010; Lioumbas and Karapantsios, 2012a, 2012b; van Koerten et al., 2015). According to these authors, the French fry crust thickness ranged from 0.4 to 1.5 mm. To overcome this problem, the porosity of the French fry crust was determined by peripheral French fry zones at depths of 0-0.2, 0.2-0.5, 0.5-0.7 and 0.7-1.0 mm from the French fry surface (Figure 1 b and c). An example of a 0.5 mm thick crust zone analysed is shown in Figure 1 b). When a large and fixed thickness of the crust zone is considered, this may include some empty area, which is located between the crust and the core. This zonal analysis does not provide information on the real thickness of the crust, but it provides information on the microstructure for each crust thickness considered. The microstructure of the selected fry zones is characterised by their porosity and pore size distribution.

Figure 4 shows the evolution of the local porosity in different parts of the crust (distances from the potato surface) as a function of water loss. It should be noted (results not shown) that the porosity before frying is 25.53% in the 0 to 0.2 mm zone, 8% between 0.2 and 0.5 mm and almost 0% in the more internal zones. It is found that increasing water loss increases the porosity of the crust in any part of the crust. At the beginning of frying, the porosity of the peripheral zone of the crust is more important than that of most internal parts. This is due to the existing porosity in the pre-crust, which has already formed because of the pretreatment of the frozen French fries. This higher porosity in the peripheral area compared to that in the internal zones can be explained by the presence of an evaporation front commonly observed during frying. The same observations were reported by van Koerten et al. (2015). At 25% water loss, the porosities of the different parts of the crust are almost identical ($\varepsilon = 35\% — 40\%$). Above 25% water loss, the porosity of the internal parts (0.5 to 1 mm) become significantly higher (P value > 0.5) than that of the peripheral part (0 to 0.2 mm) (Figure 4). In this peripheral part of the crust, the porosity ranges from 35 to 45%, 40 to 50%

265 and 35 to 40% for water losses of 37.5, 50 and 60%, respectively, while the porosity ranges
266 from 55 to 65%, 60 to 78% and 60 to 75% for water losses of 35.5, 50 and 60%, respectively,
267 for part of the inner part of the crust (0.5 to 0.7 mm from the surface). However, regardless of
268 the frying process used, the local porosity in the different parts of the crust is not significantly
269 different (P value > 0.05) for the same water loss. From a water loss of 37.5%, the porosity of
270 the different parts of the crust increase slightly (increases of 5 — 8% and 1 — 5% for water
271 losses of 50% and 60%, respectively). Other authors reported a similar evolution of the crust
272 porosity at the end of frying for different fried foods such as potato strips (Krokida et al.,
273 2000), tortilla chips (Kawas and Moreira, 2001) and sweet potatoes (Taiwo and Baik, 2007).

274 3.4. Pore size distribution in a crust

275 An analysis of morphometric parameters was carried out on the French fry crusts with a
276 thickness of 1 mm. Figure 5 illustrates the evolution of morphometric parameters such as the
277 median diameter (d_{50}) and span in the first millimeter of the French fries (0 to 1 mm) as a
278 function of water loss. The analysis in Figure 5 a) shows that in the first millimeter of the
279 French fries, the median pore diameter of the hot-air fries is larger than that of the deep-fat
280 fries. Beyond 37.5% water loss, this difference in median pore diameter becomes very
281 significant (P value < 0.05); deep-fat frying generates a median pore diameter smaller than 0.2
282 mm in this first millimetre (0 to 1 mm) of the French fry, whereas it is higher than 0.2 mm for
283 hot-air frying. It is also found that the size of the largest pores of the deep-fat fries ranges
284 from 0.15 mm to 0.5 mm for 50% water loss and from 0.18 mm to 0.6 mm for 60% water
285 loss. For the same water losses, the largest pore sizes of the hot-air fries range from 0.3 mm to
286 0.7 mm and 0.4 mm to 0.8 mm, respectively. For the same total porosity created in the crust
287 (figure 4), the pore size distribution depends on the frying process. In figure 5 b), the span
288 evolution is plotted as a function of water loss. The span of the deep-fat fries decreases
289 slightly from 3 to 2.5 as the water loss increases, whereas for the hot-air fries, the span in the

first millimeter decreases significantly (P value < 0.05) from approximately 3 to 1.5 as the water loss increases. For French fries with a water loss greater than 37.5%, the span of the deep-fat fries is significantly (P value < 0.05) higher than that of the hot-air fries. The pore size distribution of the deep-fat fries is therefore more heterogeneous than that of the hot-air fries for the same water loss. Deep-fat frying generates smaller pore diameters and a heterogeneous pore size distribution in the first millimeter of the crust, while hot-air frying generates larger pores and a more homogeneous pore size distribution. However, it is important to note that the difference in the pore diameter distribution (V_p[0 to 0.15 mm], d_{50} and span) observed between the hot-air fries and deep-fat fries decreases when the crust thickness considered is lower (0.7 mm or 0.5 mm).

3.5. Local distribution of pore sizes

The pore size distribution was obtained by measuring the pore sizes in the volume of interest of 500 stacks of French fry crusts (Figure 1). Figure 6 shows the cumulative percentages of the pore size distributions in different parts of the crusts of hot-air fries and deep-fat fries. The pore diameter globally increases from the surface to the core of the fry for the same water loss. The first 0.2 mm of the crust of the hot-air and deep-fat fries have small pore diameters (for WL= 50%, d_{50} = 0.08 mm and for WL= 60%, d_{50} = 0.05 mm) compared to the deeper parts of the crust. Vauvre et al. (2014) also found that pore diameter increased moving away from the surface of the fry. The median diameter of the pore in the crust from 0.5 to 0.7 mm of the surface increases with water loss, while the median pore diameter in the crust from 0 to 0.2 mm does not change significantly. The structure of this peripheral part does not appear to evolve as a function of water loss.

Through comparison of the pore size distributions of the hot-air fries and deep-fat fries for the same water loss (Figure 6), it is found that the pore size of the hot-air fries is larger than that of deep-fat fries in the different parts of the crust except for the first 0.2 mm. For

example, for deep-fat fries with water loss of 50%, the median pore sizes in the different parts of the crust (0 to 0.2, 0.2 to 0.5, 0.5 to 0.7 and 0.7 to 1 mm) are 0.08, 0.1, 0.3 and 0.5 mm, respectively. For hot-air fries with the same water loss (50%), the pore diameter varies in the different parts of the crust from 0.09, 0.18, 0.38 and 0.6, respectively. The difference between the pore diameters of the hot-air fries and deep-fat fries is not significant (P value > 0.5) in the first 0.2 mm of the crust. Nevertheless, it is significantly (P value < 0.5) higher in the deeper parts of the crust. The difference in the frequency of the pore diameter distribution between the hot-air fries and deep-fat fries may be associated with transfer phenomena in the French fries during frying. In fact, deep-fat frying is a process of heat and water transfer that causes fast water evaporation from food. In contrast to deep-fat frying, hot-air frying induces a lower heat and mass transfer with a heat transfer coefficient $h < 100$ W.m^{-2}. K^{-1} and an evaporation flux density < 4 .10^{-3} kg.m^{-2}.s^{-1} (Andrés et al., 2013; Teruel et al., 2015). The high heat and mass transfer intensity in deep-fat frying ($150 < h < 1500$ W.m^{-2}. K^{-1} and an evaporation flux density > 5.10^{-3} kg.m^{-2}.s^{-1}) (Costa et al., 1999; Vitrac et al., 2002; Vitrac and Trystram, 2005) lead to faster dehydration of the surface of the fry, which becomes rigid and can oppose the water evaporation fluxes. This generates an overpressure that can reach 30 kPa in French fries during deep-fat frying (Li et al., 2011; Patsioura et al., 2016; Vauvre et al., 2014). A high intensity of transfers can therefore generate high pressure on the structure of the potatoes and create a high number of small-sized pores in the crust. Van Koerten et al. (2015) also showed that the higher transfer intensity permitted a larger evaporation zone inside French fries and allowed the creation of a higher number of small-sized pores but also a very heterogeneous pore size distribution. On the other hand, the lower intensity of heat and water transfer in the case of hot-air frying could lead to a slower creation of new pores and be more favourable to the growth of the first pores created. Overpressure data are not available in the literature, but this parameter can be expected to be lower for hot-air frying. Van Loon (2005) indicated that

340 the low overpressure induced by hot-air frying was insufficient to cause the cell separation
341 necessary for a more distributed porosity.

342 ### 3.6. Morphometric parameters *versus* sensory and instrumental textures

343 The samples in Table 1 marked with an asterisk * were characterized by sensory and
344 instrumental texture analysis; the data were obtained from the research of Gouyo et al. (2020)
345 (crispiness of the crust, product hardness, softness of the core and flouriness of the core). The
346 data show that the deep-fat fries were crispier than the hot-air fries, and those with 60% water
347 loss (BH180_60) were the crispiest of all the samples. The data showed that the acoustic
348 parameter NSP (number of sound peaks) ($r = 0.89$; P-value < 0.01) was strongly positively
349 correlated with the crispness of the crust and that the mechanical (penetration test) parameter
350 Fmax (maximum force) was strongly correlated with the product hardness ($r = 0.9$;
351 P value < 0.01). In Figure 7, a relationship is established between the morphometric
352 parameters of the first millimeter of the crust of the French fries and the sensory
353 descriptors and instrumental texture parameters by principal component analysis (PCA). The
354 PCA shows that 96.90% of the variability could be explained by the first two main
355 components: 58.25% by the first component F1 and 38.65% by the second component F2.
356 The morphometric parameters are projected as supplementary variables and do not influence
357 the principal components of the analysis. The first dimension (F1 axis) is built by the
358 contributions of the following variables: product hardness (28.06%), softness of the
359 core (23.91%), floury of the core (20.30%) and Fmax (24.58%), which are highly correlated
360 with this axis ($|r| > 0.84$). The second axis (F2 axis) is built by the crispiness of the
361 crust (43.03) and the NSP (38.13), which are very highly correlated with this axis ($r > 0.94$).
362 The bi-plot (Figure 7) indeed illustrates that deep-fat fried products (DF180_60 and
363 DF180_50) are associated with the highest values of the sensory crispiness of the crust and of
364 the NSP. The crispiness of the crust and NSP are indeed strongly positively correlated, with a

correlation coefficient r = 0.94 (P value < 0.05). On the first axis, the hot-air fried product with 60% water loss (AY180_60), which was considered the hardest and not crispy by Gouyo et al. (2020), is related to higher values of product hardness, floury of the core and Fmax.

The span of the pore size distribution and the volume of pores with low diameters (V_p[0 to 0.15] and V_p[0.32 to 0.5]) appear highly and positively correlated with axis 2 (r = 0.84, 0.87 and 0.86, respectively), while d_{50} and the volume of the large pores are negatively correlated with this axis (r = – 0.71 and – 0.87, respectively). The crispiness of the crust thus increases when small pores are formed but decrease when large pores are formed; the crispness of the crust and NSP are indeed significantly (P value < 0.05) positively correlated to the span and the volume of pores with diameters ranging from 0 to 0.15 mm. These correlations do not appear, however, to be linear (Figure 8). The median diameter (d_{50}) is poorly (P value < 0.10) anti-correlated with the crispiness of the crust, but the regression appears to be more linear. This relationship between small pores and crispness corresponds to what is expected because according to Vincent, (1998), Thanatuksorn et al. (2007) and Gouyo et al. (2020), a high number of force peaks and sound peaks (NSP) corresponds to a higher fracturability of the crust. These peaks basically represent numerous small fracture incidents during deformation (van Koerten et al., 2015). It is therefore considered that the more small pores are present in the first millimetre (0 to 1 mm) of a French fry instead of large pores, the more small incidents of fracture occur during deformation of the French fry.

For axis 1, the total porosity (ε) appears positively correlated with this axis and with the floury of the core (r = 0.88, P value < 0.05). As the porosity increases, the floury of the core increases. This could be explained by the fact that a high-water loss of the product leads to a very porous product and a very dry core that gives the sensation of flouriness.

These results showed that the increase in the span of the pore size distribution and the volume of the pores with diameters ranging from 0 to 0.15 mm (V_p[0 to 0.15]) and the

390 decrease in the d_{50} are favourable to a good crispness of the fried product. The results show
391 that crispness is not the consequence of a single morphometric parameter but a combination
392 of microstructures generated in the crust. To have a good level of crispness in fried products,
393 heterogeneous pore sizes with median diameters smaller than 0.2 mm must therefore be
394 generated in the first millimetre of the product crust.

395 ## 4. Conclusion

396 The microstructure development of the crust of French fries obtained by hot-air and
397 deep-fat frying was analysed with XMT. The results showed that the prefrozen French fries
398 do not practically undergo any volume shrinkage during frying (deep-fat or hot-air frying). It
399 is shown that the total porosity created in French fries is proportional to the water loss during
400 frying, regardless of the frying process. The French fries obtained by hot-air frying mainly
401 differ from those obtained by deep-fat frying through a larger mean pore diameter. Principal
402 component analysis (PCA) between the sensory, instrumental and morphometric parameters
403 of the first millimeter of the French fry correlates the microstructure of the crust developed
404 during frying with the crispness of the crust. To have a good level of crispness in fried
405 products, the frying process must generate heterogeneous pores with a high volume of pores
406 with diameters ranging from 0 to 0.15 mm and median diameter smaller than 0.2 mm in the
407 first millimetre of the crust.
408
409
410
411
412
413
414

Table 1: French fry sample conditions obtained by deep fat frying (DF) or air frying (AY) at two different temperatures (for oil bath or air) and six different water loss levels.

Sample code	Frying equipment	T °C	Water loss (% i.m.)
DF180_5	Deep-Fat Fryer	180	5.0
DF180_12.5	Deep-Fat Fryer	180	12.5
DF180_25	Deep-Fat Fryer	180	25.0
DF180_37.5	Deep-Fat Fryer	180	37.5
DF180_50 *	Deep-Fat Fryer	180	50.0
DF180_60 *	Deep-Fat Fryer	180	60.0
AY180_5	Air Fryer	180	5.0
AY180_12.5	Air Fryer	180	12.5
AY180_25	Air Fryer	180	25.0
AY180_37.5	Air Fryer	180	37.5
AY180_50 *	Air Fryer	180	50.0
AY180_60 *	Air Fryer	180	60.0
AY200_50 *	Air Fryer	200	50.0

Samples marked with an asterisk (*) correspond to samples used for sensory analysis according to the data from Gouyo et al. (2020). i.m. corresponds to the initial mass.

5. Acknowledgements

This study was funded by SEB Group, ANRT "Agence National de la Recherche et de la Technologie" and CIRAD-Montpellier. We would like to express our thanks to Léa Ollier, Laboratory Technician at QualiSud UMR, for his assistance.

6. References

Adedeji, A.A., Liu, L., Ngadi, M.O., 2011. Microstructural evaluation of deep-fat fried chicken nugget batter coating using confocal laser scanning microscopy. J. Food Eng. 102, 49–57. https://doi.org/10.1016/j.jfoodeng.2010.08.002

Adedeji, A.A., Ngadi, M.O., 2011. Microstructural Characterization of Deep-Fat Fried Breaded Chicken Nuggets Using X-Ray Micro-Computed Tomography. J. Food Process Eng. 34, 2205–2219. https://doi.org/10.1111/j.1745-4530.2009.00565.x

Aguilera, J.M., 2005. Why food microstructure? J. Food Eng., IV Iberoamerican Congress of Food Engineering (CIBIA IV) 67, 3–11. https://doi.org/10.1016/j.jfoodeng.2004.05.050

Alam, T., Takhar, P.S., 2016. Microstructural Characterization of Fried Potato Disks Using X-Ray Micro Computed Tomography. J. Food Sci. 81, E651–E664. https://doi.org/10.1111/1750-3841.13219

Altamirano-Fortoul, R., Le-Bail, A., Chevallier, S., Rosell, C.M., 2012. Effect of the amount of steam during baking on bread crust features and water diffusion. J. Food Eng. 108, 128–134. https://doi.org/10.1016/j.jfoodeng.2011.07.015

Andrés, A., Arguelles, Á., Castelló, M.L., Heredia, A., 2013. Mass Transfer and Volume Changes in French Fries During Air Frying. Food Bioprocess Technol. 6, 1917–1924. https://doi.org/10.1007/s11947-012-0861-2

Besbes, E., Jury, V., Monteau, J.-Y., Le Bail, A., 2013. Characterizing the cellular structure of bread crumb and crust as affected by heating rate using X-ray microtomography. J. Food Eng. 115, 415–423. https://doi.org/10.1016/j.jfoodeng.2012.10.005

Borgefors, G., 1996. On Digital Distance Transforms in Three Dimensions. Comput. Vis. Image Underst. 64, 368–376. https://doi.org/10.1006/cviu.1996.0065

Bouchon, P., Aguilera, J.M., 2001. Microstructural analysis of frying potatoes. Int. J. Food Sci. Technol. 36, 669–676. https://doi.org/10.1046/j.1365-2621.2001.00499.x

460 Costa, R.M., Oliveira, F.A.R., Boutcheva, G., 2001. Structural changes and shrinkage of
461 potato during frying. Int. J. Food Sci. Technol. 36, 11–23.
462 https://doi.org/10.1046/j.1365-2621.2001.00413.x
463 Costa, R.M., Oliveira, F.A.R., Delaney, O., Gekas, V., 1999. Analysis of the heat transfer
464 coefficient during potato frying. J. Food Eng. 39, 293–299.
465 https://doi.org/10.1016/S0260-8774(98)00169-1
466 Dalen, G.V., Nootenboom, P., Vliet, L.J.V., Voortman, L., Esveld, E., 2007. 3-D imaging,
467 analysis and modelling of porous cereal products using x-ray microtomography. Image
468 Anal. Stereol. 26, 169–177. https://doi.org/10.5566/ias.v26.p169-177
469 Du, C.-J., Sun, D.-W., 2006. Automatic measurement of pores and porosity in pork ham and
470 their correlations with processing time, water content and texture. Meat Sci. 72, 294–
471 302. https://doi.org/10.1016/j.meatsci.2005.07.016
472 Feldkamp, L.A., Davis, L.C., Kress, J.W., 1984. Practical cone-beam algorithm. JOSA A 1,
473 612–619. https://doi.org/10.1364/JOSAA.1.000612
474 Ferrando, M., Spiess, W.E.L., 2000. Review: Confocal scanning laser microscopy. A
475 powerful tool in food science. Food Sci. Technol. Int. 6, 267–284.
476 https://doi.org/10.1177/108201320000600402
477 Gouyo, T., Mestres, C., Maraval, I., Fontez, B., Hofleitner, C., Bohuon, P., 2020. Assessment
478 of acoustic-mechanical measurements for texture of French fries: Comparison of deep-
479 fat frying and air frying. Food Res. Int. 131, 108947.
480 https://doi.org/10.1016/j.foodres.2019.108947
481 Hafsa, I., Cuq, B., Kim, S.J., Le Bail, A., Ruiz, T., Chevallier, S., 2014. Description of
482 internal microstructure of agglomerated cereal powders using X-ray microtomography
483 to study of process–structure relationships. Powder Technol. 256, 512–521.
484 https://doi.org/10.1016/j.powtec.2014.01.073
485 Hesso, N., Garnier, C., Loisel, C., Chevallier, S., Bouchet, B., Le-Bail, A., 2015. Formulation
486 effect study on batter and cake microstructure: Correlation with rheology and texture.
487 Food Struct. 5, 31–41. https://doi.org/10.1016/j.foostr.2015.03.002
488 Hildebrand, T., Rüegsegger, P., 1997. A new method for the model-independent assessment
489 of thickness in three-dimensional images. J. Microsc. 185, 67–75.
490 https://doi.org/10.1046/j.1365-2818.1997.1340694.x
491 Horigane, A.K., Motoi, H., Irie, K., Yoshida, M., 2003. Observation of the Structure,
492 Moisture Distribution, and Oil Distribution in the Coating of Tempura by NMR Micro

493 Imaging. J. Food Sci. 68, 2034–2039. https://doi.org/10.1111/j.1365-
494 2621.2003.tb07014.x
495 Hullberg, A., Ballerini, L., 2003. Pore formation in cured-smoked pork determined with
496 image analysis - effects of tumbling and RN- gene. Meat Sci. 65, 1231–1236.
497 https://doi.org/10.1016/S0309-1740(03)00030-5
498 Kaláb, M., Allan-Wojtas, P., Miller, S.S., 1995. Microscopy and other imaging techniques in
499 food structure analysis. Trends Food Sci. Technol. 6, 177–186.
500 https://doi.org/10.1016/S0924-2244(00)89052-4
501 Kassama, L.S., Ngadi, M.O., 2005. Pore structure characterization of deep-fat-fried chicken
502 meat. J. Food Eng. 66, 369–375. https://doi.org/10.1016/j.jfoodeng.2004.04.003
503 Kawas, M.L., Moreira, R.G., 2001. Effect of Degree of Starch Gelatinization on Quality
504 Attributes of Fried Tortilla Chips. J. Food Sci. 66, 300–306.
505 https://doi.org/10.1111/j.1365-2621.2001.tb11336.x
506 Krokida, M.K., Oreopoulou, V., Maroulis, Z.B., 2000. Effect of frying conditions on
507 shrinkage and porosity of fried potatoes. J. Food Eng. 43, 147–154.
508 https://doi.org/10.1016/S0260-8774(99)00143-0
509 Laverse, J., Mastromatteo, M., Frisullo, P., Del Nobile, M.A., 2011. X-ray microtomography
510 to study the microstructure of cream cheese-type products. J. Dairy Sci. 94, 43–50.
511 https://doi.org/10.3168/jds.2010-3524
512 Léonard, A., Blacher, S., Nimmol, C., Devahastin, S., 2008. Effect of far-infrared radiation
513 assisted drying on microstructure of banana slices: An illustrative use of X-ray
514 microtomography in microstructural evaluation of a food product. J. Food Eng. 85,
515 154–162. https://doi.org/10.1016/j.jfoodeng.2007.07.017
516 Li, Y., Mason, G., Morrow, N.R., Ruth, D.W., 2011. Capillary Pressure at a Saturation Front
517 During Restricted Counter-Current Spontaneous Imbibition with Liquid Displacing
518 Air. Transp. Porous Media 87, 275–289. https://doi.org/10.1007/s11242-010-9681-x
519 Lioumbas, J.S., Karapantsios, T.D., 2012a. Effect of Potato Orientation on Evaporation Front
520 Propagation and Crust Thickness Evolution during Deep-Fat Frying. J. Food Sci. 77,
521 E297–E305. https://doi.org/10.1111/j.1750-3841.2012.02915.x
522 Lioumbas, J.S., Karapantsios, T.D., 2012b. Evaporation Front Compared with Crust
523 Thickness in Potato Deep-Fat Frying. J. Food Sci. 77, E17–E25.
524 https://doi.org/10.1111/j.1750-3841.2011.02472.x

Lorensen, W.E., Cline, H.E., 1987. Marching cubes: A high resolution 3D surface construction algorithm. ACM SIGGRAPH Comput. Graph. 21, 163–169. https://doi.org/10.1145/37402.37422

Lucas, T., Collewet, G., Bousquières, J., Deligny, C., 2018. The size of eye-shaped bubbles in Danish pastry in relation to the size of fat fragments; A reverse engineering approach of the alveolar structure. J. Food Eng. 237, 194–203. https://doi.org/10.1016/j.jfoodeng.2018.04.025

Miranda, M.L., Aguilera, J.M., 2006. Structure and Texture Properties of Fried Potato Products. Food Rev. Int. 22, 173–201. https://doi.org/10.1080/87559120600574584

Otsu, N., 1979. A Threshold Selection Method from Gray-Level Histograms. IEEE Trans. Syst. Man Cybern. 9, 62–66. https://doi.org/10.1109/TSMC.1979.4310076

Patsioura, A., Vauvre, J.-M., Kesteloot, R., Smith, P., Trystram, G., Vitrac, O., 2016. Chapter 17 - Mechanisms of Oil Uptake in French Fries, in: Singh, J., Kaur, L. (Eds.), Advances in Potato Chemistry and Technology (Second Edition). Academic Press, San Diego, pp. 503–526. https://doi.org/10.1016/B978-0-12-800002-1.00017-0

Pedreschi, F., 2009. Fried and Dehydrated Potato Products. pp. 319–337. https://doi.org/10.1016/B978-0-12-374349-7.00011-8

Pedreschi, F., Aguilera, J.M., 2002. Some Changes in Potato Chips During Frying Observed by Confocal Laser Scanning Microscopy (CLSM). Food Sci. Technol. Int. 8, 197–201. https://doi.org/10.1106/108201302027931

Pinthus, E.J., Weinberg, P., Saguy, I.S., 1995. Deep-Fat Fried Potato Product Oil Uptake as Affected by Crust Physical Properties. J. Food Sci. 60, 770–772. https://doi.org/10.1111/j.1365-2621.1995.tb06225.x

Primo-Martín, C., van Dalen, G., Meinders, M.B.J., Don, A., Hamer, R.H., van Vliet, T., 2010. Bread crispness and morphology can be controlled by proving conditions. Food Res. Int. 43, 207–217. https://doi.org/10.1016/j.foodres.2009.09.030

Rahman, M.S., Al-Amri, O.S., Al-Bulushi, I.M., 2002. Pores and physico-chemical characteristics of dried tuna produced by different methods of drying. J. Food Eng. 53, 301–313. https://doi.org/10.1016/S0260-8774(01)00169-8

Remy, E., Thiel, E., 2002. Medial axis for chamfer distances: computing look-up tables and neighbourhoods in 2D or 3D. Pattern Recognit. Lett., Discrete Geometry for Computer Imagery 23, 649–661. https://doi.org/10.1016/S0167-8655(01)00141-6

557 Salvador, A., Varela, P., Sanz, T., Fiszman, S.M., 2009. Understanding potato chips crispy
558 texture by simultaneous fracture and acoustic measurements, and sensory analysis.
559 LWT - Food Sci. Technol. 42, 763–767. https://doi.org/10.1016/j.lwt.2008.09.016
560 Taiwo, K.A., Baik, O.D., 2007. Effects of pre-treatments on the shrinkage and textural
561 properties of fried sweet potatoes. LWT - Food Sci. Technol. 40, 661–668.
562 https://doi.org/10.1016/j.lwt.2006.03.005
563 Teruel, M. del R., Gordon, M., Linares, M.B., Garrido, M.D., Ahromrit, A., Niranjan, K.,
564 2015. A Comparative Study of the Characteristics of French Fries Produced by Deep
565 Fat Frying and Air Frying. J. Food Sci. 80, E349–E358. https://doi.org/10.1111/1750-
566 3841.12753
567 Thanatuksorn, P., Kajiwara, K., Suzuki, T., 2007. Characterization of deep-fat frying in a
568 wheat flour–water mixture model using a state diagram. J. Sci. Food Agric. 87, 2648–
569 2656. https://doi.org/10.1002/jsfa.3027
570 van Koerten, K.N., Schutyser, M.A.I., Somsen, D., Boom, R.M., 2015. Crust morphology and
571 crispness development during deep-fat frying of potato. Food Res. Int. 78, 336–342.
572 https://doi.org/10.1016/j.foodres.2015.09.022
573 Vauvre, J.-M., Kesteloot, R., Patsioura, A., Vitrac, O., 2014. Microscopic oil uptake
574 mechanisms in fried products. Eur. J. Lipid Sci. Technol. 116, 741–755.
575 https://doi.org/10.1002/ejlt.201300278
576 Vickers, Z., Bourne, M.C., 1976. Crispness in Foods-a Review. J. Food Sci. 41, 1153–1157.
577 https://doi.org/10.1111/j.1365-2621.1976.tb14406.x
578 Vincent, J.F.V., 1998. The quantification of crispness. J. Sci. Food Agric. 78, 162–168.
579 https://doi.org/10.1002/(SICI)1097-0010(199810)78:2<162::AID-JSFA97>3.0.CO;2-3
580 Vitrac, O., Dufour, D., Trystram, G., Raoult-Wack, A.-L., 2002. Characterization of heat and
581 mass transfer during deep-fat frying and its effect on cassava chip quality. J. Food
582 Eng. 53, 161–176. https://doi.org/10.1016/S0260-8774(01)00153-4
583 Vitrac, O., Trystram, G., 2005. A method for time and spatially resolved measurement of
584 convective heat transfer coefficient (h) in complex flows. Chem. Eng. Sci. 60, 1219–
585 1236. https://doi.org/10.1016/j.ces.2004.09.046
586 Yamsaengsung, R., Moreira, R.G., 2002. Modeling the transport phenomena and structural
587 changes during deep fat frying: Part I: model development. J. Food Eng. 53, 1–10.
588 https://doi.org/10.1016/S0260-8774(01)00134-0
589 Yan, G., Tian, J., Zhu, S., Dai, Y., Qin, C., 2008. Fast cone-beam CT image reconstruction
590 using GPU hardware. J. X-Ray Sci. Technol. 16, 225–234.

591 Ziaiifar, A.M., Courtois, F., Trystram, G., 2010. Porosity Development and Its Effect on Oil
592 Uptake During Frying Process. J. Food Process Eng. 33, 191–212.
593 https://doi.org/10.1111/j.1745-4530.2008.00267.x
594

a) **b)** **c)**

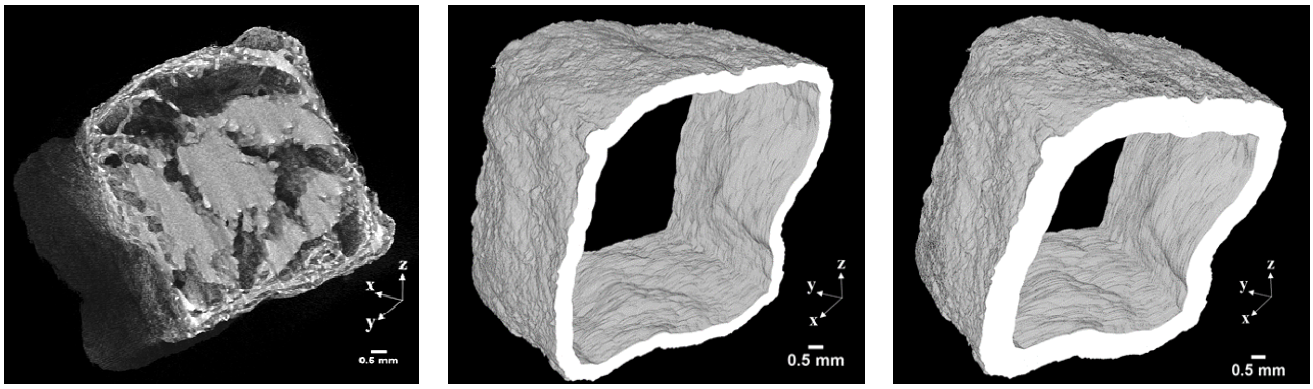

Figure 1: 3D image of a) the global French fry obtained from XMT of hot-air frying and French fry with an ROI corresponding to crusts b) 0.5 mm thick and c) 1 mm thick.

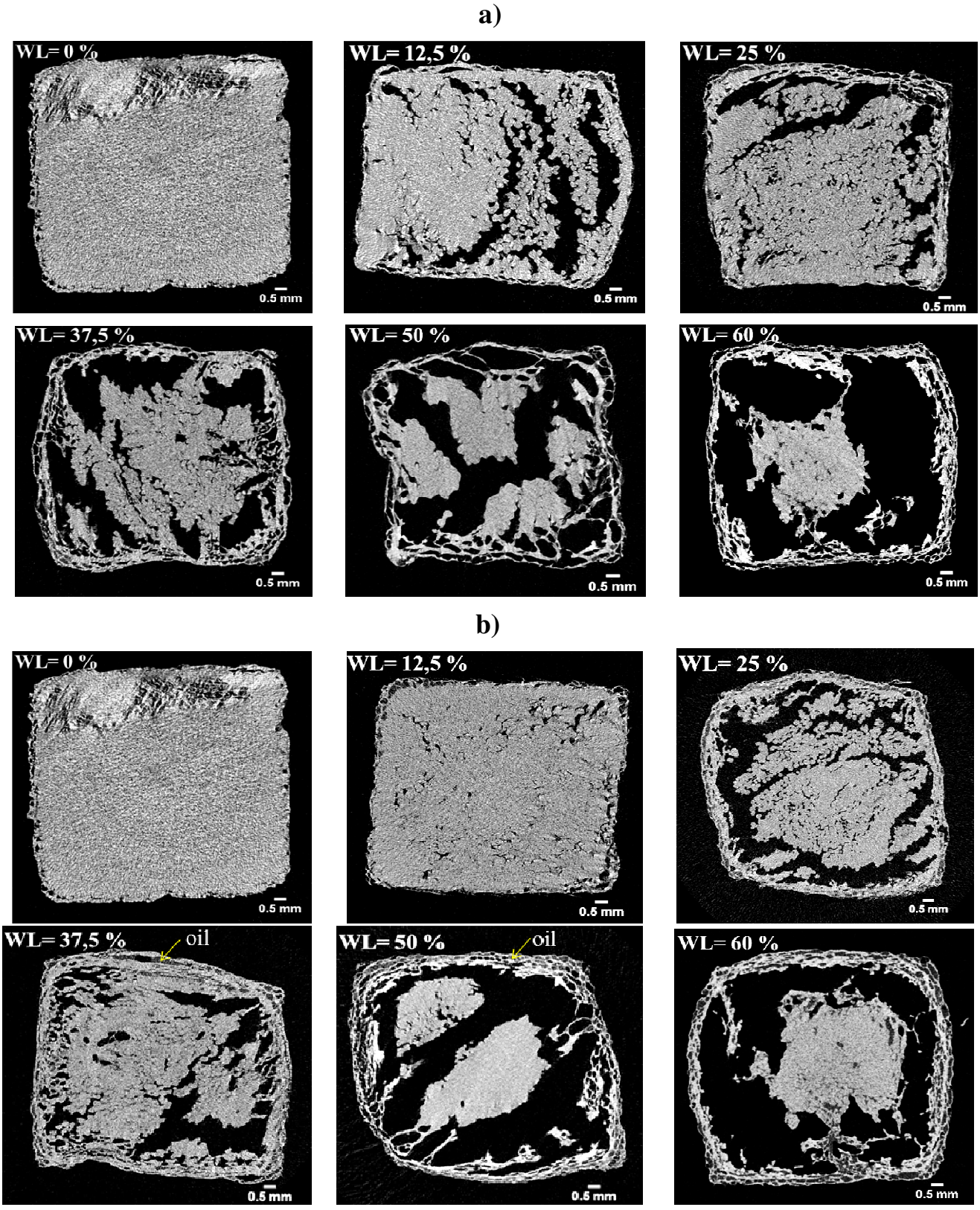

Figure 1: Cross-sectional slices (2D images) obtained from X-ray micro-computed tomography of **a**) hot-air fries and **b**) deep-fat fries as a function of water loss (WL) expressed in kg of water per kg of initial mass.

The square section was preserved during frying, and the porosity of the fries increased with increasing water loss.

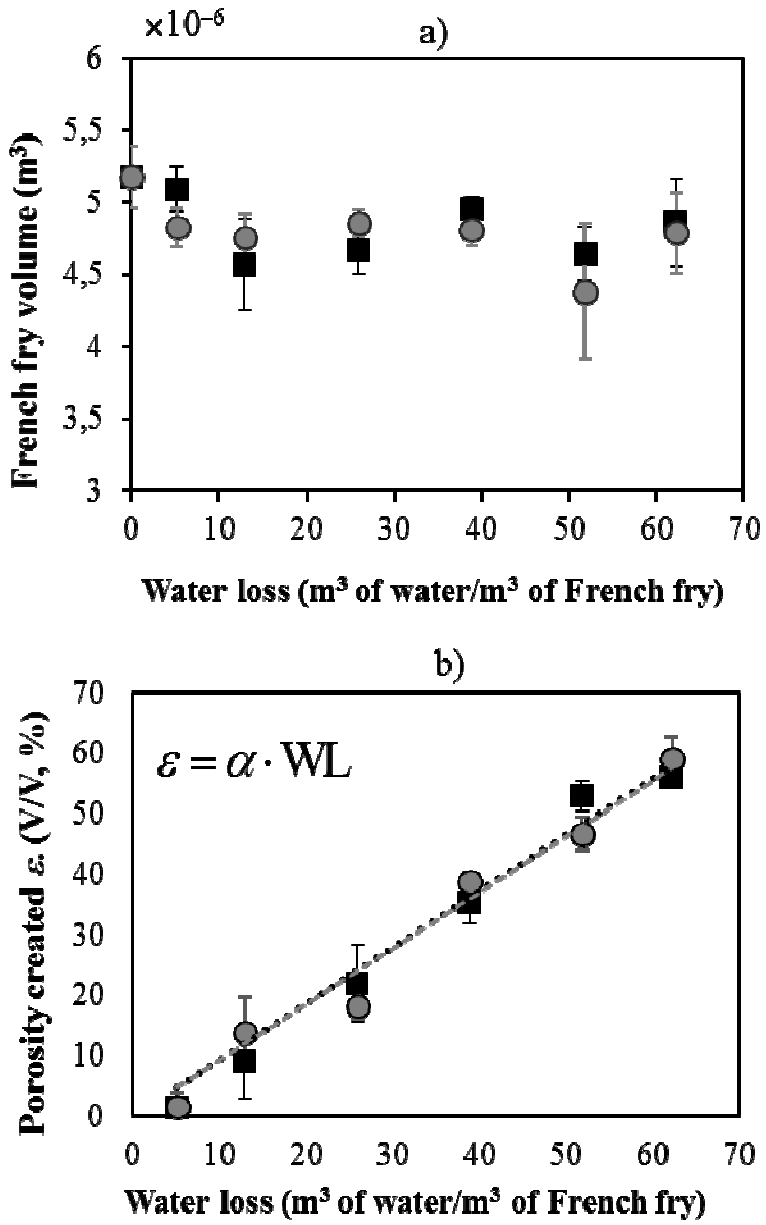

Figure 1: a) Volume change in hot-air frying (●) and deep-fat frying (■) and b) total porosity created (ε) as a function of water loss (WL). The dashed line represents the linear regression of hot-air frying ($\alpha = 0.92 \pm 0.15$ with $R^2 = 0.98$) and deep-fat frying ($\alpha = 0.93 \pm 0.13$ with $R^2 = 0.98$). Error bars represent the standard deviation between replicates.

Figure 3a highlights a low volume shrinkage of French fries during frying. The porosity created in the fry increases proportionally to the water loss and independently of the frying conditions (Figure 3 b).

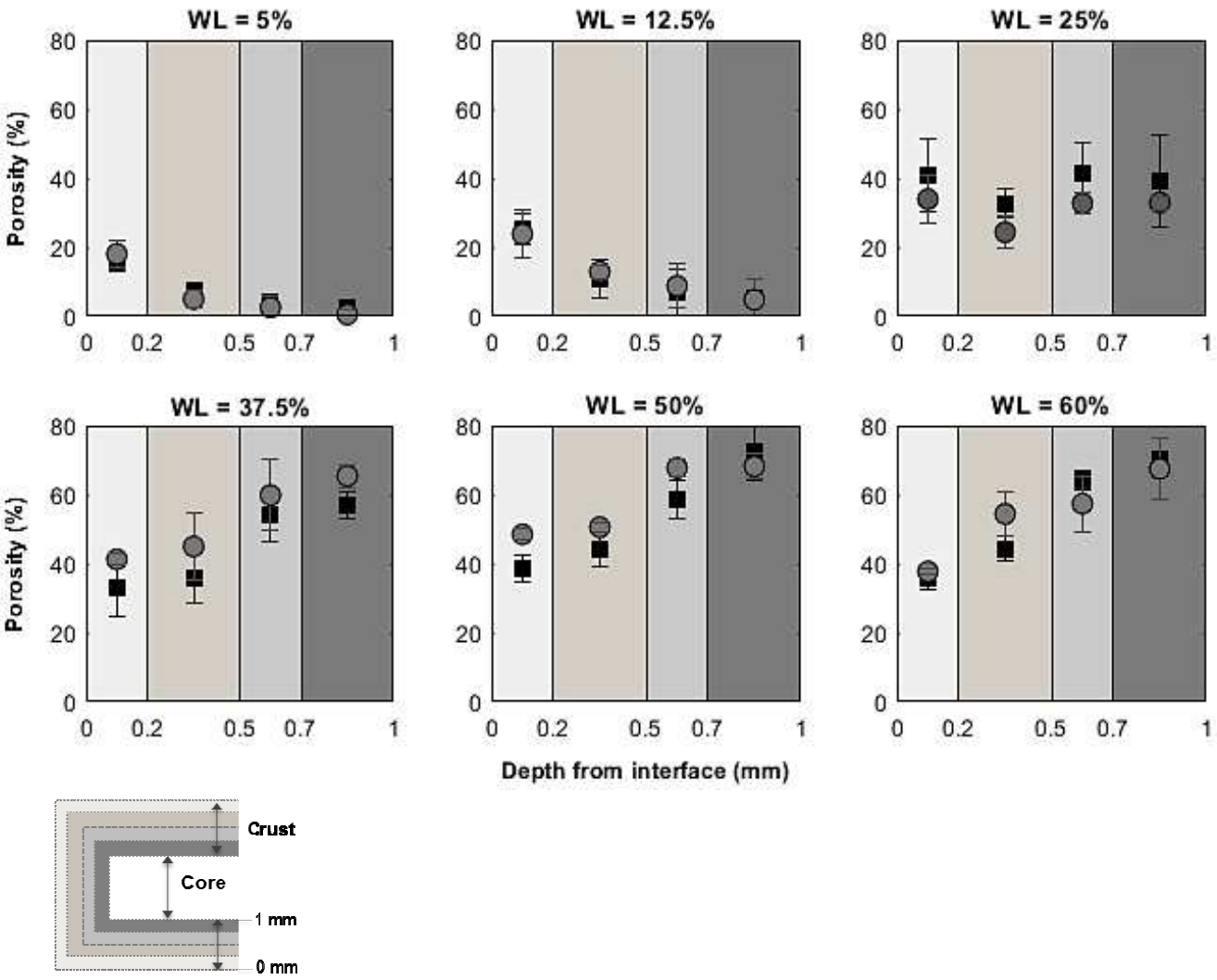

Figure 1: Evolution of the local porosity created in different parts of the crust as a function of water loss (WL) for hot-air French fries (●) and deep-fat French fries (■). Error bars represent the standard deviation between replicates.

Increasing water loss increases the porosity of the crust in any part of the crust. In each part of the crust, the local porosity created by the two types of frying process was not significantly different (P value > 0.05) for the same water loss.

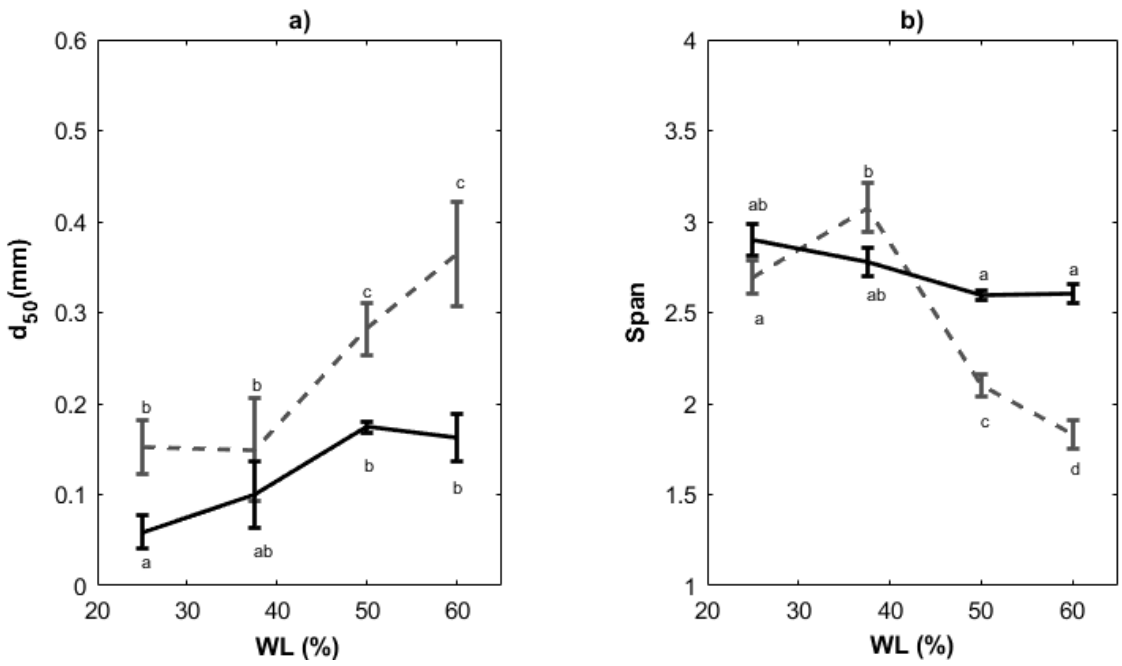

Figure 1: Evolution of the a) median diameter (d_{50}) and b) heterogeneity of the pore size distribution (span) in 1 mm of crust as a function of water loss for hot-air fries (---) and deep-fat fries (—). The marks with the same superscript (a–d) do not differ significantly (Fisher LSD test, P value ≤ 0.05). Error bars represent the standard deviation between replicates.

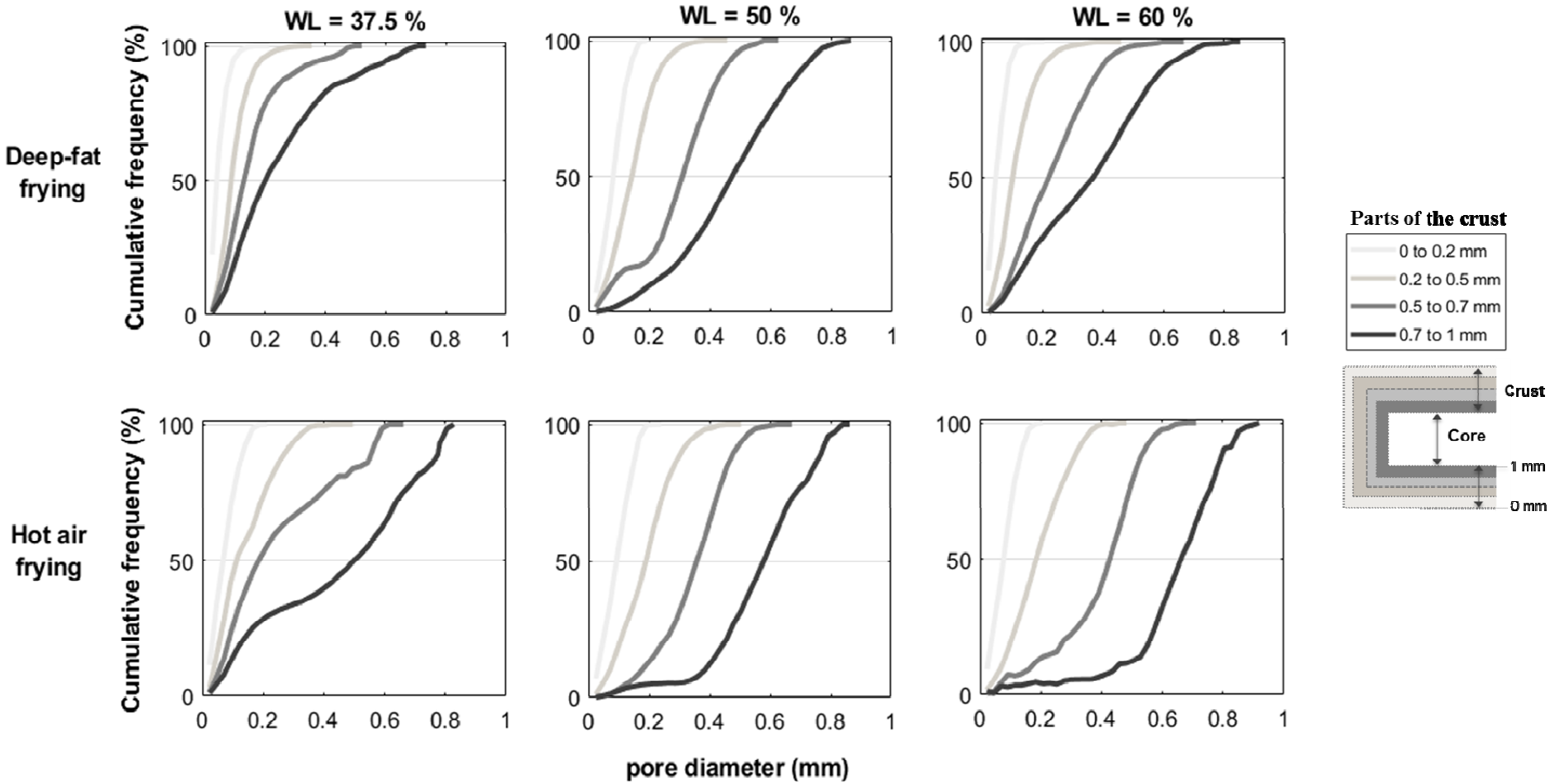

Figure 1: Pore diameter distribution in different parts of the crust during hot-air frying and deep-fat frying for different water loss (WL).

The pore diameter globally increases from the surface to the core of the fry for the same water loss. The pore size of the hot-air fries is larger than that of deep-fat fries in the different parts of the crust except for the first 0.2 mm.

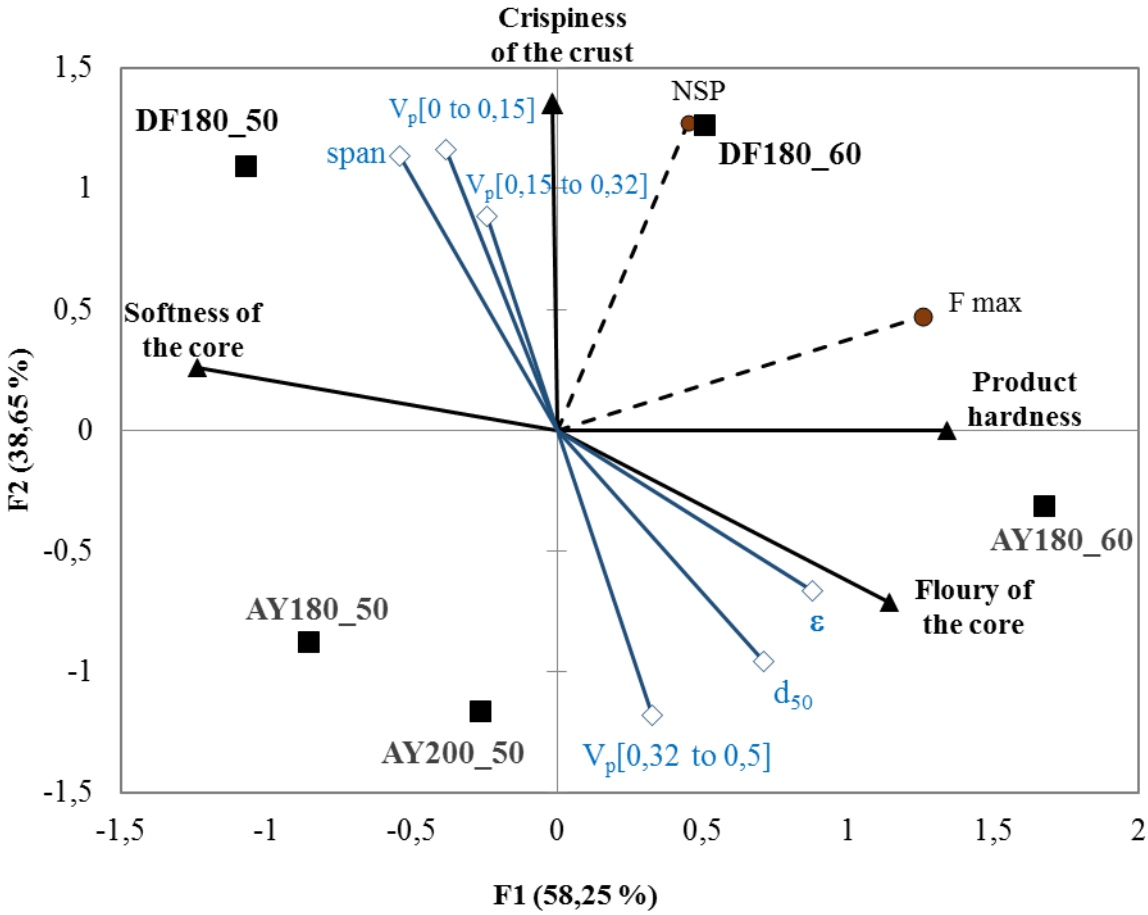

Figure 1: Bi-plot of PCA regarding sensory descriptors (▲) according to (Gouyo et al., 2019), instrumental data (●) according to (Gouyo et al., 2019) and microstructure parameter (□) dataset for French fry samples (■) obtained by deep-fat frying (DF) or air frying (AY) at different temperatures (180 and 200 °C) and different water loss levels of 50 and 60% (i.m.).

V_p[0 to 0,15] = volume of pores with diameter ranging from 0 to 0.15 mm.

V_p[0.15 to 0.32] = volume of pores with diameter ranging from 0.15 to 0.32 mm.

V_p[0.32 to 0.5] = volume of pores with diameter ranging from 0.32 to 0.5 mm.

ε = total porosity

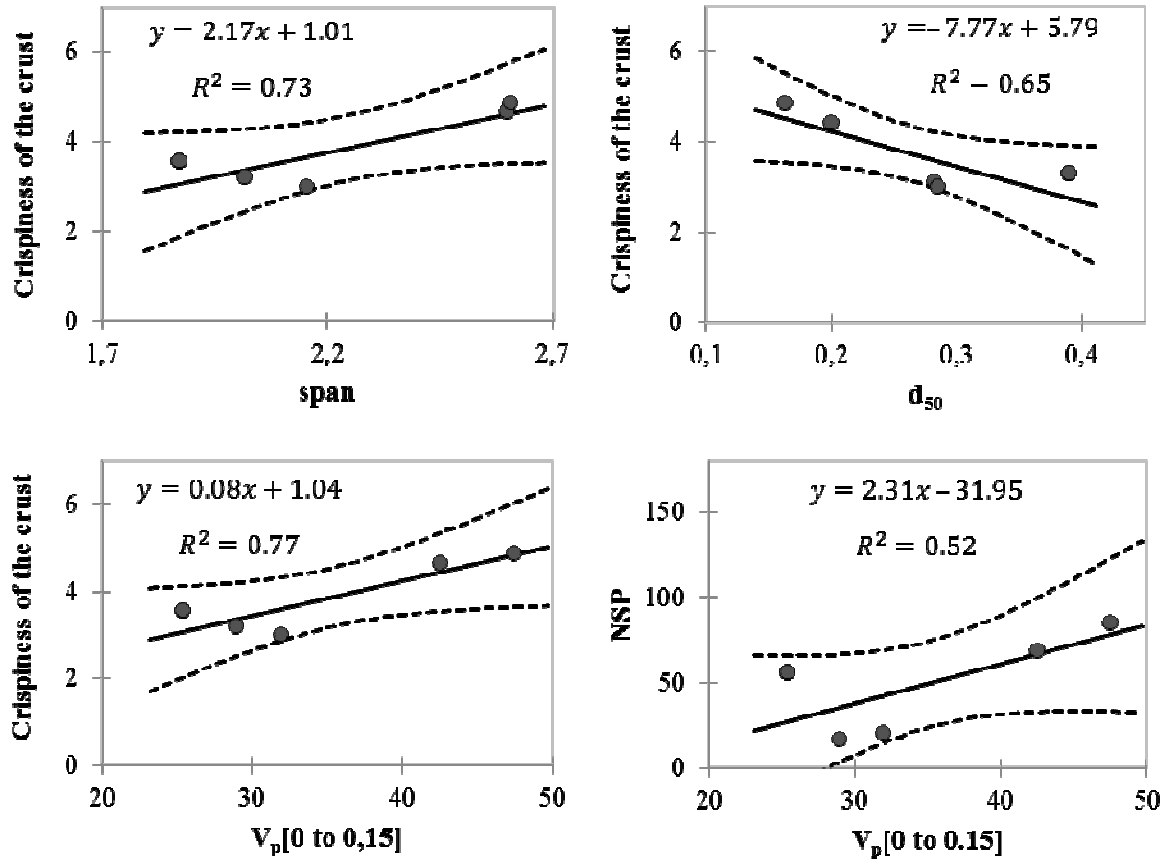

Figure 1: Linear regression (solid line) between sensory descriptors ($y =$ crispiness of the crust) and microstructure parameters ($x =$ span, d_{50} and V_p[0 to 0,15]) and between the number of sound peaks ($y =$ NPS) and $x = V_p$[0 to 0,15]. 95% confidence interval (dashed line). Vp[0 to 0,15] represents the volume of pores with diameter ranging from 0 to 0.15 mm.